J Mol Model (2012) 18:2543–2551
DOI 10.1007/s00894-011-1261-7

ORIGINAL PAPER

Ab initio and DFT study of luminescent cyclometalated N-heterocyclic carbene organogold(III) complexes

Baozhu Yang · Qi Zhang · Jing Zhong · Shuang Huang · Hong-Xing Zhang

Received: 12 April 2011 / Accepted: 27 September 2011 / Published online: 27 October 2011

Abstract The structures of versatile N-heterocyclic carbene-containing Au(III) complexes in the ground and low-lying excited states have been optimized at the B3LYP functional and the single-excitation configuration interaction (CIS) method, respectively. The spectral properties are predicted with time-dependent density functional theory (TDDFT). In addition, the charge transport quality has been estimated approximately by the predicted reorganization energy (λ). As revealed from the calculations, the introduction of methyl has a bigger influence on the spectral properties than phenyl. Furthermore, we find that changing the auxiliary ligand could tune the charge transfer properties.

Keywords *Ab initio* · Absorption and emission spectrum · DFT · Gold(III) complexes · N-heterocyclic carbene

Introduction

Traditionally, carbenes were considered to be unstable, short-lived, electron-deficient two-coordinated carbon compounds with two non-bonding electrons. Until 1968, Öfele [1] and Wanzlick [2] first reported the use of N-heterocyclic carbenes (NHCs) as ligands independently. The singlet NHCs are stabilized by the interaction of the empty p-orbital with the two neighboring nitrogen lone pairs [3]. Earlier work considered NHCs as phosphine analogues [4, 5], but the recent observations emphasized some differences in steric and electronic properties and their chemical behavior [6–8]. Since these ligands act as excellent strong σ-donors, they can produce stable metal−NHCs with strong metal−carbon bonds [9–11]. At present NHCs are common and powerful ligands in organometallic chemistry. A number of metal−NHCs complexes have been applied in catalysis [12–14] and pharmaceutical fields [15, 16].

Au atom with $5d^{10}6s^{1}$ electronic structure exhibits very strong relativistic effects. For phosphorescent complex, the strong spin-orbit coupling effect of Au atom increases the rate of $S_1 \rightarrow T_1$ intersystem crossing, then the phosphorescence originating from the triplet excited states can be achieved. In recent years, Au(I) complexes have been the subject of some studies, such as the application in medical chemistry, catalysis, biophysical, photophysical and photochemical properties [17–20]. In contrast to the Au(I) system, most of the Au(III) complexes usually emit at low temperature in the solid state or glasses, with very few examples emitting at room temperature in solution [21]. One probable reason for the behavior in Au(III) complexes is the presence of low-energy radiationless d−d states [21], which compete with the charge transfer transition and result in weak- or non-luminescence at room temperature. The key to raising the energy of the d−d states is to introduce strong-field ligands or co-ligands [22]. So the NHCs ligands attracted much attention, due to the strong σ-donating ability. Recently, Nolan and Huynh reported the synthesis of Au(III)-NHC complexes by oxidative addition [23, 24]. Later on, Yam and co-workers synthe-

Electronic supplementary material The online version of this article (doi:10.1007/s00894-011-1261-7) contains supplementary material, which is available to authorized users.

B. Yang · Q. Zhang · J. Zhong (✉)
School of Petrochemical Engineering, Changzhou University, Changzhou 213100, Jiangsu, People's Republic of China
e-mail: zjwyz@cczu.edu.cn

S. Huang · H.-X. Zhang
State Key Laboratory of Theoretical and Computational Chemistry, Institute of Theoretical Chemistry, Jilin University, Changchun 130023, People's Republic of China

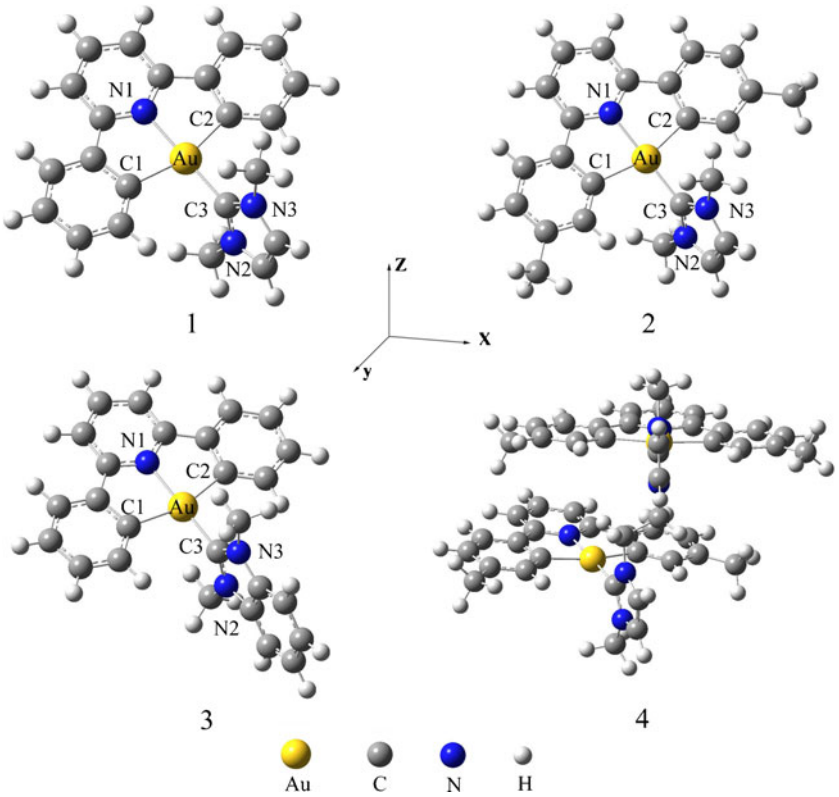

Fig. 1 Optimized ground state structures for 1–4 by the DFT (B3LYP) calculations

sized a series of mononuclear and dinuclear luminescent NHC-containing organogold(III) complexes [25]. In contrast to previously reported Au(III)-NHC complexes, which were synthesized through the oxidative addition reactions of their Au(I)-precursor complexes, the preparation of such NHC-containing cyclometalated Au(III) complexes involves the direct incorporation of NHC into the Au(III) starting materials. These complexes display long-lived emission and high luminescent efficiency.

Although there have been some reports about the photophysical and photochemical properties of Au(III)-NHC complexes, corresponding theoretical research works are sparse. Herein, a detailed theoretical investigation on the electronic structures and spectra of the complexes 1–4 (Fig. 1) was undertaken under the *ab initio* and the density functional theory (DFT) level. We hope the exploration of these characteristic properties for the Au(III)-NHC complexes would help us to design good phosphorescent materials.

Table 1 Partial optimized geometric structural parameters of 1–4 in S_0 and T_1 states, together with the experimental values of 1

	1			2		3		4	
Parameters	S_0	T_1	exptl[a]	S_0	T_1	S_0	T_1	S_0	T_1
Bond lengths (Å)									
Au−C1	2.109	2.078	2.054	2.110	2.078	2.108	2.078	2.108	2.086
Au−C2	2.107	2.078	2.151	2.110	2.078	2.108	2.078	2.112	2.091
Au−C3	2.024	2.044	1.999	2.025	2.045	2.028	2.048	2.028	2.043
Au−N1	2.036	1.994	1.975	2.035	1.993	2.036	1.993	2.033	2.008
Bond angles (deg)									
C1−Au−C2	161.4	162.3	160.9	161.4	162.2	161.4	162.2	161.4	162.4
N1−Au−C3	180.0	180.0	179.4	180.0	180.0	180.0	180.0	177.3	177.2
Dihedral angle (deg)									
C1−Au−C3−N2	77.1	85.4		74.1	85.2	89.5	89.5	90.7	92.9

[a] From ref [25]

Table 2 Partial molecular orbital compositions (%) in the ground states for 1–3 in CH_2Cl_2 solution under TD-DFT (B3LYP) calculations

			1			
MO	*E* (eV)		Au	C^N^C	NHC	Bond type
L+2	−1.6624	$28.8d_{x^2-y^2}$		48.9	22.3	d(Au)+π*(C^N^C)+σ*(NHC)
L+1	−1.9560			98.4		π*(C^N^C)
L	−2.5402	$5.3d_{z^2}$		93.3		π*(C^N^C)
Δ_{H-L}=4.0058 eV						
H	−6.5487	$8.2d_{yz}$		90.6		π(C^N^C)
H−1	−6.9229	$5.5d_{yz}$		70.3	24.2	π(C^N^C)+π(NHC)
H−2	−7.1153	$6.5d_{yz}$		90.7		π(C^N^C)
H−3	−7.2718			98.6		π(C^N^C)
			2			
MO	*E* (eV)		Au	C^N^C	NHC	Bond type
L+2	−1.6534	$28.6d_{x^2-y^2}$		45.1	22.3	d(Au)+π*(C^N^C)+σ*(NHC)
L+1	−1.9021			98.1		π*(C^N^C)
L	−2.5043	$6.4d_{z^2}$		92.9		π*(C^N^C)
Δ_{H-L}=3.8844 eV						
H	−6.3887	$5.2d_{yz}$		93.5		π(C^N^C)
H−1	−6.9134	$6.9d_{yz}$		76.7	16.4	π(C^N^C)+π(NHC)
H−2	−7.0372			98.6		π(C^N^C)
H−3	−7.1009	$8.7d_{yz}$		90.0		π(C^N^C)
			3			
MO	*E* (eV)		Au	C^N^C	NHC	Bond type
L+2	−1.7320	$29.3d_{x}2_{-y}2$		48.1	22.6	d(Au)+π*(C^N^C)+σ*(NHC)
L+1	−1.9617			99.5		π*(C^N^C)
L	−2.5636	$7.6d_{z^2}$		89.8		π*(C^N^C)
Δ_{H-L}=3.9947 eV						
H	−6.5583	$4.3d_{yz}$		95.7		π(C^N^C)
H−1	−6.9123	$10.4d_{yz}$		62.6	27.0	d(Au)+π(C^N^C)+π(NHC)
H−2	−7.1180	$7.7d_{yz}$		91.2		π(C^N^C)
H−3	−7.2258				99.1	π(NHC)
H−4	−7.2807			98.7		π(C^N^C)
H−5	−7.4092			98.3		π(C^N^C)

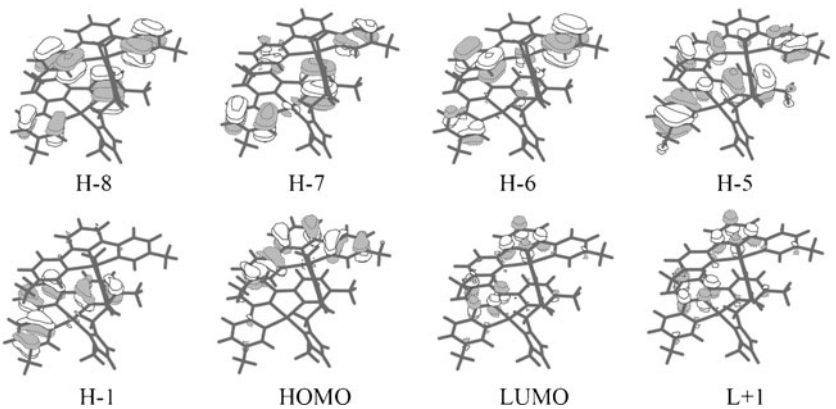

Fig. 2 Molecular orbital diagrams of 4 in the ground state

Table 3 Absorptions of 1–4 in CH_2Cl_2 solution according to TD-DFT calculations, together with the experimental values

		Excitation[a] (coeff)	E_{nm} (eV)	Oscillator	Assignment	exptl (nm)[b]
1	S_1	H→L (0.68)	380 (3.27)	0.0559	ILCT	386
	S_2	H−1→L (0.69)	346 (3.59)	0.0014	ILCT/LLCT	369
	S_3	H−2→L (0.67)	313 (3.96)	0.1539	ILCT	
	S_5	H−3→L (0.65)	301 (4.12)	0.0555	ILCT	
2	S_1	H→L (0.68)	392 (3.16)	0.0860	ILCT	396
	S_2	H−1→L (0.68)	344 (3.61)	0.0021	ILCT/LLCT	378
	S_5	H−3→L (0.67)	313 (3.97)	0.1380	ILCT	
	S_6	H→L+1 (0.50)	302 (4.10)	0.1886	ILCT	
3	S_1	H→L (0.68)	381 (3.25)	0.0550	ILCT	387
	S_2	H−1→L (0.67)	345 (3.59)	0.0012	ILCT/LLCT	369
	S_3	H−2→L (0.67)	314 (3.94)	0.1562	ILCT	
	S_5	H−4→L (0.65)	302 (4.10)	0.0599	ILCT	
	S_6	H−5→L (0.46)	299 (4.14)	0.0802	ILCT	
		H→L+1 (0.45)				
4	S_1	H→L (0.51)	397 (3.13)	0.0568	ILCT/LLCT	400
	S_2	H−1→L (0.49)	394 (3.15)	0.0783	ILCT/LLCT	
	S_3	H→L+1 (0.56)	365 (3.39)	0.0027	ILCT/LLCT	382
	S_4	H−1→L+1 (0.56)	363 (3.41)	0.0029	ILCT/LLCT	
	S_{10}	H−6→L (−0.37)	316 (3.92)	0.0264	ILCT	
		H−5→L (0.47)				
	S_{12}	H−7→L (0.45)	314 (3.95)	0.1210	ILCT	
	S_{20}	H−5→L+1 (0.45)	302 (4.11)	0.1836	ILCT	
		H−8→L+1 (−0.35)				
	S_{22}	H−7→L+1 (0.46)	300 (4.12)	0.0351	ILCT	
		H−6→L+1 (−0.24)				

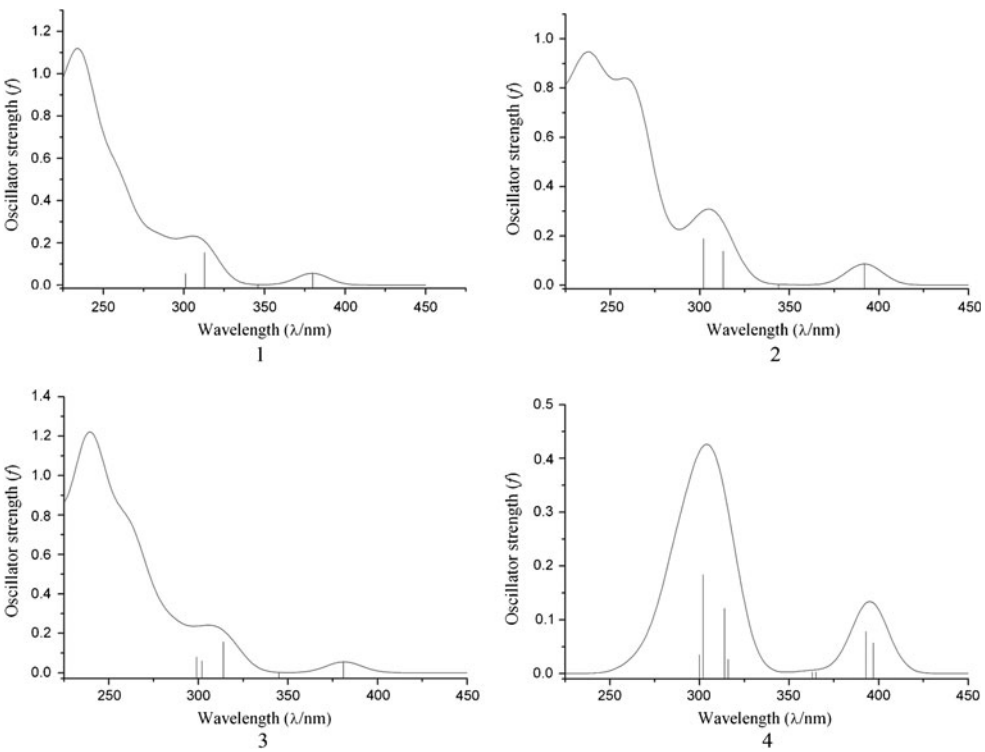

Fig. 3 Simulated absorption spectra of 1–4 in CH_2Cl_2 solution

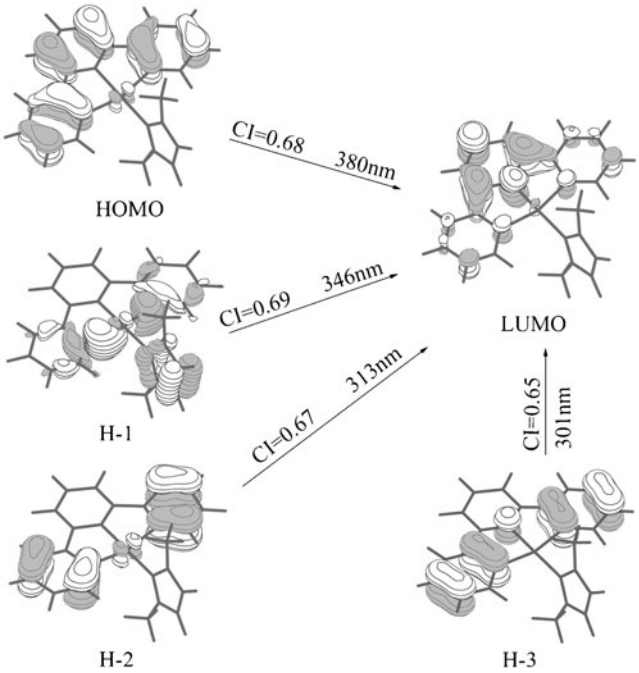

Fig. 4 Single electron transitions with the maximum CI coefficients under TD-DFT calculations for the 380, 346, 313 and 301 nm absorptions of 1 in dichloromethane

Computational details and theory

The density functional theory (DFT) at the Becke's three parameter functional and the lee-Yang-Parr functional (B3LYP) [26–29] and single-excitation configuration interaction (CIS) method [30, 31] are employed to optimize the ground (S_0) and excited state (T_1) structures without symmetry constrains for 1–4, respectively. As we known, CIS method is successful in the structure optimization of the excited state proved by many researchers [32, 33]. However, the transition energies obtained by the CIS calculations are usually overestimated since the CIS method uses the orbitals of a HF state in an ordinary CI procedure to solve for the higher roots and only considered parts of the electronic correlation effects via the mixing of excited determinants [30, 31, 34]. In our work, the spectroscopic properties related to the absorption and emission in solution are obtained by the time-dependent density functional theory (TDDFT) [35–37] at the B3LYP functional associated with the polarized continuum model (PCM) [38, 39]. This kind of theoretical approach has been proven to be reliable for transition-metal complex systems [40–42].

In the work, quasi-relativistic pseudo-potentials of Au atoms proposed by Hay and Wadt [43, 44] with 19 valence electrons are employed, and the LANL2DZ basis sets associated with the pseudo-potential are adopted. The 6-31 G(d) basis sets were adopted for H, C, and N atoms. To precisely describe the molecular properties, one additional f-type polarization function is implemented for Au (α= 0.20) [45]. All the calculations are accomplished by using the Gaussian03 software package [46].

Results and discussion

The ground states structures and the absorption spectra

The optimized S_0 structures of 1–4 are depicted in Fig. 1 with the coordination axis. Complex 4 is a dinuclear molecule, which is composed by complex 2 through alkyl side chains on the carbine nitrogen atoms. For metal complex, the bond lengths and bond angles between the metal and ligands are important, which indicate the interaction between the metal and the ligand. In Table 1, the corresponding important parameters together with the X-ray crystal diffraction data of 1 are listed. As reported in Table 1, the optimized bond lengths and bond angles for 1 in the ground state are in general agreement with the corresponding experimental values. The calculated bond lengths are elongated by about 2% compared with the experimental values of 1, except for Au−C2 bond, which are shortened by 2%. There are minor differences in important parameters for 1–4 and the change of ligands has little influence upon the ground state geometries. The discrepancy of the geometry structural data between the calculated and measured values is reasonable and acceptable, since the environments of the complexes are different

Table 4 Phosphorescent emissions of 1–4 in CH_2Cl_2 solution according to TD-DFT (B3LYP) calculations, together with the experimental values

	Transition	Configuration[a]	Coeff	*E* (nm) (eV)	Assignment	exptl (nm)[b]
1	$^3A\rightarrow{}^1A$	L→H	0.72	494 (2.51)	^{3}ILCT	479
		L+1→H−2	−0.18			
2	$^3A\rightarrow{}^1A$	L→H	0.72	511 (2.43)	^{3}ILCT	489
		L+1→H−1	0.18			
3	$^3A\rightarrow{}^1A$	L→H	0.72	496 (2.50)	^{3}ILCT	480
		L+1→H−3	0.18			
4	$^3A\rightarrow{}^1A$	L→H	0.67	565 (2.19)	^{3}ILCT	493
		L+2→H	0.28			

[a] H denotes the HOMO and L the LUMO

[b] From ref 13

Table 5 Partial molecular orbital compositions in the lowest-energy excited-state for 1 in CH_2Cl_2 solution by TD-DFT calculations

			1			
MO	*E* (eV)		Au	C^N^C	NHC	Bond type
L+2	−1.4191	$28.4d_{x^2-y^2}$		48.1	23.5	d(Au)+π*(C^N^C)+σ*(NHC)
L+1	−1.9745			98.8		π*(C^N^C)
L	−2.6131	$4.9d_{z^2}$		92.8		π*(C^N^C)
HOMO−LUMO energy gap						
H	−6.4053	$5.9d_{yz}$		94.1		π(C^N^C)
H−1	−7.0108	$9.7d_{yz}$		74.7	15.6	d(Au)+π(C^N^C)+π(NHC)
H−2	−7.1735			98.6		π(C^N^C)

in the two cases: in the latter case, the molecule is in a tight crystal lattice, while in the former case, the molecule is free.

The spectral data are obtained in CH_2Cl_2 solution on experiment [25]. For comparison, we calculated the absorption spectra in CH_2Cl_2 (ξ=8.93) solution for 1–4 using the PCM model. As seen in Table 2, three conclusions can be drawn: (1) the complexes 1–3 have similar orbital composition. (2) The frontier molecular orbitals are almost localized on C^N^C (the tridentate ligand) ligands. (3) The composition of Au atomic orbitals is less than 10% in the high-energy occupied orbitals, except for the HOMO−1 (10.4%) of 3, and that in LUMO+2 of 1–3 are almost 30%. To help us understand the orbitals described above, the molecular orbital diagrams of partial frontier molecular orbitals of 4 are displayed directly in Fig. 2. From Fig. 2, we find that the HOMO and HOMO−1 of 4 have the same composition, The difference is the orbital are localized on different ligand. The rest of the frontier molecular orbital are almost localized on the C^N^C ligands. As Table 3 shows, the calculated data agree well with the experimental value. So the PCM model is suitable for our system. It is well known that the frontier molecular orbitals play a major role in the electronic transition, so we first reveal the frontier molecular orbitals for 1–3.

Table 3 gives the absorption data in terms of the transition states, excitation energies, excitations with maximum CI coefficients, oscillator strengths for 1–4 in CH_2Cl_2 solution, and the experimental values of 1–4. For clarity, we list in Table 3 only the most leading excited states. Furthermore, we simulated the absorption spectra of 1–4 with a Gaussian-type curve in Fig. 3. As revealed in Table 3, the lowest-lying dipole-allowed absorptions (S_1) are at 380, 392, 381, and 397 nm for 1–4, respectively, in which the leading excitation configuration of HOMO→LUMO is responsible for the transitions. The experimental values are 386, 396, 387, and 400 nm, respectively. The calculated result is reasonable and acceptable. From Table 2, we know the HOMOs of 1–3 are almost composed of π(C^N^C), while the LUMO are composed of π*(C^N^C). So the lowest-lying absorptions are attributed to intra-ligand charge transfer (ILCT). In Fig. 2, we can see the LUMO of 4 is composed of π*(C^N^C), which is localized on two ligands. The HOMO is localized on π(C^N^C) of one ligand. So the transition is assigned as ILCT combined with ligand-to-ligand charge transfer (LLCT). With respect to S_2 excited state of 1–4, the leading excitation configuration is HOMO−1→LUMO transition. Table 2 and Fig. 2 show that the HOMO−1 of 1–3 are all composed of π(C^N^C) and π(NHC), so the transitions are assigned as ILCT and LLCT. The rest of the calculated absorptions of 1–4 are shown in Table 3. To intuitively understand the absorptions of 1 in solution, we display the molecular orbital diagrams in Fig. 4, in which four single electron excitations corresponding to the CI coefficients are involved.

The lowest-energy absorptions of 1–3 are red-shifted in the order 1, 3<2. From Table 2, we can see the HOMO−LUMO energy gaps of 1 (4.0058 eV) and 3 (3.9947 eV) are higher than 2 (3.8844 eV). Comparison with complex 1, with the electron-donating ability of C^N^C ligand increasing

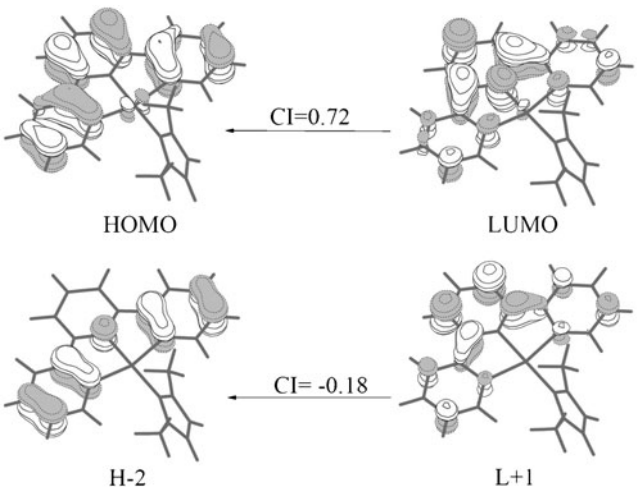

Fig. 5 Single-electron transitions according to TD-DFT calculations for the 494 nm emission of 1 in CH_2Cl_2 solution

Table 6 The dipole moment of 1–4 in S_0 and T_1 states

μ (Debye)				
	1	2	3	4
S_0	3.2698	3.6033	0.9927	6.9592
T_1	3.8749	3.9940	1.5396	7.1447
Δμ	0.6051	0.3907	0.5469	0.1855

in 2, the energy level of HOMO and LUMO are all elevated, but the LUMO increase is much smaller than HOMO. This is because the LUMO composition has less change than HOMO composition. Then the HOMO−LUMO energy gap of 2 is less than that of 1. In complex 3 the phenyl was introduced into NHC ligand, then the electron-withdrawing ability of NHC ligand is increased. The energy level of HOMO and LUMO are all reduced, and the degree is the same. So there is little difference between 1 and 3 in the HOMO−LUMO energy gap. Then the lowest-energy absorptions of 2 is red-shifted relative to that of 1, 3.

We also find an interesting phenomenon in Fig. 3. The absorption band of 4 appears in pairs, such as 397 nm, 394 nm and 365 nm, 363 nm. From Table 3 and Fig. 2, we can find each of them have the same transition character. The difference is that the molecular orbital of the transitions result from different ligands.

The excited states structures and the emission spectra

On the basis of the optimized ground state structures, the lowest-energy excited state structures of 1–4 are fully optimized by the CIS method. The main geometry parameters of 1–4 in the lowest triplet excited state are presented in Table 1. As shown in Table 1, the main geometry parameters have a minor change compared to those of ground states, a general shortening of bond lengths between Au(III) and C^N^C ligands for 1–4 are observed. The distance between Au(III) and NHCs are lengthened. The dihedral angle between C^N^C ligand and NHC ligand increased obviously for 1–4. These show the interaction between the Au(III) atom and NHC ligands was weakened upon excitation. In order to obtain the convincing emissive energy, based on the excited state structures optimized by the CIS method, the emission spectra of 1–4 in CH_2Cl_2 solution are calculated by the TD-DFT approach at the B3LYP level. The corresponding emissions of 1–4 are listed in Table 4, associated with the emission energies, transition assignments, and the experimental values. To conveniently discuss the transition property of emission, the partial frontier molecular orbital compositions of 1 are presented in Table 5, which of 2 and 3 are displayed in Table S1.

The calculated emissions in CH_2Cl_2 solution are 494, 511, 496, and 565 nm, respectively. The results are in general agreement with the corresponding experimental values, with the exception of 4. The phosphorescent emissions are all assigned to ^{3}ILCT characters. As seen from Table 4, the 494 nm emission of 1 is assigned to the phosphorescent emission arising from the $^3A \rightarrow {}^1A$ transition and the excitation LUMO→HOMO has the largest configuration coefficient (0.72). In Table 5 we can see that the LUMO of 1 is composed of 92.8% π*(C^N^C), while the HOMO is mainly localized on 94.1% π(C^N^C). Therefore, the emission is assigned as ^{3}ILCT character. To intuitively understand the nature of the emissions, diagrams of the single-electron transitions related to the phosphorescence of 1 are shown in Fig. 5. Similar to that, as seen in Table S1, the HOMO and LUMO of 2 and 3 have similar compositions with that in 1. So the emission of 2 and 3 are also assigned as ^{3}ILCT characters. The calculated emission of 4 is 565 nm, which deviates from experimental value of 493 nm. The reason may be that the CIS method has a large error on calculating dinuclear large molecule.

We also calculated the dipole moment of 1–4 in ground states and excited states and the data are listed in Table 6. In ground states, complex 4 has the biggest dipole moment, since it is a dinuclear molecule. Complex 3 has the smallest dipole moment because the conjugation effect of NHC ligand is increased compared to complex 1. In excited states, the dipole moment of 1–4 are all increased and complex 1 and 3 increased more than the others. The reason may be the transitions occurred in C^N^C ligand with ^{3}ILCT characters and complex 1 and 3 have the same C^N^C structure.

Ionization potentials and electron affinities

As we know, the injection and transport capability of electron and hole are very important for the luminescent material. So we discuss the change tendency of the charge

Table 7 Ionization potentials (IPs), electronic affinities (EAs) and reorganization energy λ (ev) for the complexes

	IP(v)	IP(a)	HEP	EA(v)	EA(a)	EEP	λ_{hole}	$\lambda_{electron}$
1	10.2424	10.1472	10.0492	3.5321	3.6518	3.7606	0.1932	0.2285
2	9.9050	9.8071	9.7064	3.4395	3.5511	3.6545	0.1986	0.2150
3	10.1581	10.0710	9.9812	3.5239	3.6736	3.7879	0.1769	0.2640
4	11.3146	11.0724	10.9309	5.5348	5.6872	5.8069	0.3837	0.2721

transfer rates for these complexes by DFT method. The energy barriers for the injection of electrons and holes are evaluated by the ionization potential (IP) and EA electron affinity (EA). The reorganization energy (λ) is used to approximately estimate the charge transport rate and balance. The IPs and EAs are obtained with both vertical (v, at the geometry of the neutral molecule) and adiabatic (a, optimized structures for both the neutral and charged molecule). Hole extraction potentials (HEP) and electron extraction potentials (EEP) are used to evaluate the extraction potentials for hole and electron, respectively. All these calculated results are given in Table 7. The calculated details are similar as those given by Refs [47–49]. By means of the hopping-type mechanism [50–52] and Marcus theory [53–55], it is known that the efficient charge transfer is mostly dominated by the value of reorganization energy which can be evaluated by the following relations [50]:

$$\begin{aligned}\lambda_{hole} &= \lambda_0 + \lambda_+ = [E^+(M) - E^+(M^+)] + [E(M^+) - E(M)] \\ &= [E^+(M) - E(M)] - [E^+(M^+) - E(M^+)] \\ &= IP(v) - HEP\end{aligned} \quad (1)$$

$$\begin{aligned}\lambda_{electron} &= \lambda_0 + \lambda_- = [E^-(M) - E^-(M^-)] + [E(M^-) - E(M)] \\ &= [E(M-) - E - (M-)] - [E(M) - E - (M)] \\ &= EEP - EA(v)\end{aligned} \quad (2)$$

where E, E^+ and E^- represent the energies of the neutral, cation and anion, respectively, and M, M^+ and M^- represent the geometries of neutral, cation and anion, respectively. As is known that a smaller IP value makes the hole injection easier, while a larger EA value makes the electron injection easier. As shown in Table 7, the values of λ_{hole} increase from 0.1769 eV to 0.3837 eV and $\lambda_{electron}$ increase from 0.2150 eV to 0.2721 eV. It is obvious that complex 3 is the best hole transfer material with the smallest λ_{hole} value. Complex 2 is the best electron transfer material with the smallest $\lambda_{electron}$ value. The balance between λ_{hole} and $\lambda_{electron}$ of complex 2 is the best of all these investigated complexes. Summing up above information, we can find that changing the auxiliary could tune the charge transfer properties.

Conclusions

The present work theoretically investigated the geometry structures, absorptions, and emission properties of four cyclometalated NHC−Au(III) complexes. The calculation reveals that the lowest-energy absorptions of 1–3 are attributed to ILCT transitions and that of 4 is ILCT/LLCT transitions, whereas the lowest-energy emissions are assigned as ^{3}ILCT character. For complex 2, the introduction of methyl has a significant impact on HOMO, and then the HOMO−LUMO energy gap of 2 is less than that of 1. For complex 3, the phenyl has little effect on HOMO−LUMO energy gap. Complex 3 is the best hole transfer material with the smallest λ_{hole} value. Complex 2 is the best electron transfer material with the smallest $\lambda_{electron}$ value. The balance between λ_{hole} and $\lambda_{electron}$ of complex 2 is the best of all these investigated complexes.

Acknowledgments This work is supported by the Scientific and technological achievements transformation and industrialization plan of Changzhou City (Innovation Funds) (CC20110003), Science and Technology Support Program of Jiangsu Province (Social Development) (BE2011651), Major Projects of Natural Science Research of Colleges and universities in Jiangsu Province (11KJA610002), the Basic Research Program of Jiangsu Natural Science Foundation (BK2011240), the Priority Academic Program Development of Jiangsu Higher Education Institutions (PAPD), and Foundation of Changzhou university (ZMF1002102).

References

1. Öfele K (1968) J Organomet Chem 12:42–43
2. Wanzlick HW, Schönherr HJ (1968) Angew Chem Int Edn 7:141–142
3. Glorius F (2007) Top Organomet Chem 21:1–20
4. Herrmann WA, Mihalios D, Öfele K, Kiprof P, Belmedjahed F (1992) Chem Ber 125:1795–1799
5. Öfele K, Herrmann WA, Mihalios D, Elison M, Herdtweck E, Scherer W, Mink J (1993) J Organomet Chem 459:177–184
6. Crabtree RH (2005) J Organomet Chem 690:5451–5457
7. Barnard PJ, Wedlock LE, Baker MV, Berners-Price SJ, Joyce DA, Skelton BW, Steer JH (2006) Angew Chem Int Edn 45:5966–5970
8. Powell AB, Bielawski CW, Cowley AH (2010) J Am Chem Soc 132:10184–10194
9. Lin IJB, Vasam CS (2007) Coord Chem Rev 251:642–670
10. Chiu PL, Chen CY, Zeng JY, Lu CY, Lee HM (2005) J Organomet Chem 690:1682–1687
11. Ghadwal RS, Roesky HW, Granitzka M, Stalke D (2010) J Am Chem Soc 132:10018–10020
12. Herrmann WA (2002) Angew Chem Int Edn 41:1290–1309
13. Hahn FE, Jahnke MC (2008) Angew Chem Int Edn 47:3122–3172
14. O Brien JM, Lee KS, Hoveyda AH (2010) J Am Chem Soc 132:10630–10633
15. De Frémont P, Stevens ED, Eelman MD, Fogg DE, Nolan SP (2006) Organometallics 25:5824–5828
16. Garrison JC (2005) YoungsWJ. Chem Rev 105:3978–4008
17. Lin IJB (2005) SVasam C. Can J Chem 83:812–815
18. De Fremont P, Scott NM, Stevens ED, Ramnial T, Lightbody OC, Macdonald CLB, Clyburne JAC, Abernethy CD, Nolan SP (2005) Organometallics 24:6301–6309
19. Singh MP, Strouse GF (2010) J Am Chem Soc 132:9383–9391
20. Li RQ, Marek A, Smirnov AI, Grebel H (2008) J Chem Phys 129:095102–095108
21. Yam VWW, Cheng ECC (2008) Chem Soc Rev 37:1806–1813
22. Yam VWW, Tang RPL, Wong KMC, Cheung KK (2001) Organometallics 20:4476–4482
23. De Frémont P, Singh R, Stevens ED, Petersen JL, Nolan SP (2007) Organometallics 26:1376–1385

24. Jothibasu R, Huynh HV, Koh LL (2008) J Organomet Chem 693:374–380
25. Au VKM, Wong KMC, Zhu N, Yam VWW (2009) J Am Chem Soc 131:9076–9085
26. Becke AD (1993) J Chem Phys 98:5648–5652
27. Stevens PJ, Devlin JF, Chabalowski CF, Frisch MJ (1994) J Phys Chem 98:11623–11627
28. Becke AD (1988) Phys Rev A 38:3098–3100
29. Lee C, Wang W, Parr RG (1988) Phys Rev B 37:785–789
30. Stanton JF, Gauss J, Ishikawa N, Head-Gordon M (1995) J Chem Phys 103:4160–4174
31. Foreman JB, Head-Gordon M, Pople A (1992) J Phys Chem 96:135–149
32. Liu T, Zhang HX, Shu X, Xia BH (2007) Dalton Trans 19:1922–1928
33. Zhou X, Zhang HX, Pan QJ, Li MX, Wang Y, Che CM (2007) Eur J Inorg Chem 15:2181–2188
34. Waiters VA, Hadad CM, Thiel Y, Colson SD, Wibergy KB, Johnson PM, Foresmanl JB (1991) J Am Chem Soc 113:4782–4791
35. Dreuw A, Head-Gordon M (2005) Chem Rev 105:4009–4037
36. Tomasi J, Mennucci B, Cammi R (2005) Chem Rev 105:2999–3093
37. Jacquemin D (2009) APerpe`te E, Clofini I, Adamo C. Acc Chem Res 42:326–334
38. Cossi M, Scalmani G, Regar N, Barone V (2002) J Chem Phys 117:43–54
39. Barone V, Cossi M (1997) J Chem Phys 107:3210–3221
40. Yang BZ, Zhou X, Liu T, Bai FQ, Zhang HX (2009) J Phys Chem A 113:9396–9403
41. Zhou X, Zhang HX (2005) J Phys Chem A 109:8809–8818
42. Yang BZ, Zhou X, Liu T, Zhao GJ, Zhang HX (2009) Inorg Chim Acta 362:1209–1214
43. Wadt WR, Hay PJ (1985) J Chem Phys 82:284–298
44. Hay PJ, Wadt WR (1985) J Chem Phys 82:299–310
45. Pyykkö P, Mendizabal F (1998) Inorg Chem 37:3018–3025
46. Frisch MJ, Trucks GW, Schlegel HB et al (2004) Gaussian 03, Revision D02. Gaussian Inc. Wallingford, CT
47. Lin BC, Cheng CP, Lao ZPM (2003) J Phys Chem A 107:5241–5251
48. Curioni A, Boero M, Andreoni W (1998) Chem Phys Lett 294:263–271
49. Mott NF, Davis EA (1979) Electronic Processes in Non-Crystalline Materials, 2nd edn. Oxford University Press, Oxford
50. Reedijk JA, Marks HCF, van Bohemen SMC, Hilt O, Brom HB, Michels MAJ (1999) Synth Met 101:475–476
51. Epstein AJ, Lee WP, Prigodin VN (2001) Synth Met 117:9–13
52. Geoffrey RH, Ratner MA, Marks TJ (2005) J Am Chem Soc 127:2339–2350
53. Marcus RA (1956) J Chem Phys 24:966–978
54. Marcus RA (1964) Annu Rev Phys Chem 15:155–196
55. Marcus RA (1993) Rev Mod Phys 65:599–610